HHS Public Access

Author manuscript

Neuron. Author manuscript; available in PMC 2016 April 22.

Published in final edited form as:

Neuron. 2015 April 22; 86(2): 578–590. doi:10.1016/j.neuron.2015.03.018.

Intrinsic and Task-Dependent Coupling of Neuronal Population Activity in Human Parietal Cortex

Brett L. Foster[1,2], **Vinitha Rangarajan**[1,2], **William R. Shirer**[1,2], and **Josef Parvizi**[1,2]

[1]Laboratory of Behavioral & Cognitive Neurology, Stanford University, 300 Pasteur Drive, Stanford, CA, 94305, USA

[2]Stanford Human Intracranial Cognitive Electrophysiology Program (SHICEP), Department of Neurology & Neurological Sciences, School of Medicine, Stanford University, 300 Pasteur Drive, Stanford, CA, 94305, USA

Summary

Human neuroimaging studies have suggested that subregions of the medial and lateral parietal cortex form key nodes of a larger brain network supporting episodic memory retrieval. To explore the electrophysiological correlates of functional connectivity between these subregions, we recorded simultaneously from medial and lateral parietal cortex using intracranial electrodes in three human subjects. We observed electrophysiological co-activation of retrosplenial/posterior cingulate cortex (RSC/PCC) and angular gyrus (AG) in the high frequency broadband (HFB, or high-gamma) range, for conditions that required episodic retrieval. During resting and sleeping states, slow fluctuations (< 1 Hz) of HFB activity were highly correlated between these task-co-activated neuronal populations. Furthermore, intrinsic electrophysiological connectivity patterns matched those obtained with resting state functional magnetic resonance imaging (fMRI) from the same subjects. Our findings quantify the spatiotemporal dynamics of parietal cortex during episodic memory retrieval and provide clear neurophysiological correlates of intrinsic and task-dependent functional connectivity in the human brain.

Introduction

Episodic memory enables adaptive behavior by mediating access to past experiences, often in the service of goal-oriented tasks. While the essential role of medial temporal lobe (MTL) structures in supporting conscious memories is well documented, there is converging

Correspondence: Josef Parvizi (jparvizi@stanford.edu) or Brett L. Foster (blfoster@stanford.edu).

Author Contributions

B.L.F and J.P. designed the experiments; B.L.F. and V.R. performed the experiments; B.L.F and W.R.S analyzed the data; B.L.F and J.P wrote the manuscript. All authors commented and approved the manuscript.

The authors declare no conflict of interest.

The views presented in this work do not necessarily reflect those of the National Institutes of Health.

evidence that episodic retrieval also engages the left medial and lateral parietal cortices (MPC and LPC) (Cabeza et al., 2008; Wagner et al., 2005). More specifically, functional brain imaging studies consistently report that the retrosplenial (RSC) and posterior cingulate (PCC) cortices in the MPC, and angular gyrus (AG) in the LPC, display similar activation profiles across a variety of episodic retrieval outcomes (Cabeza et al., 2008; Wagner et al., 2005). In addition, these parietal subregions are part of a large-scale network of association cortices in the primate brain, known as the default mode network (DMN) (Greicius et al., 2003; Raichle et al., 2001; Vincent et al., 2007). As key nodes of the DMN, the RSC/PCC and AG share strong reciprocal anatomical connections and display correlated fluctuations of resting state hemodynamic activity (Greicius et al., 2003; Vincent et al., 2006).

While functional neuroimaging studies have localized the medial and lateral parietal subregions that contribute to episodic retrieval (Cabeza et al., 2008; Hutchinson et al., 2009; Vilberg and Rugg, 2008; Wagner et al., 2005), the rapid electrophysiological dynamics underlying these responses remain to be explored. Identifying the temporal sequence of activation across different parietal subregions during retrieval is essential to elucidating their unique functional role and further advancing current theoretical accounts. Moreover, the neurophysiological correlates of intrinsic and task-dependent connectivity between parietal subregions has yet to be studied. Existing data suggest that intrinsic connectivity patterns often recapitulate co-activation patterns observed during task conditions (Smith et al., 2009), possibly reflecting a shared neurophysiological correlate. Therefore, quantifying the similarities of such connectivity patterns, and their physiological correlates, is essential to understanding the neuronal basis and utility of intrinsic functional connectivity in the brain.

To specifically address these questions, we obtained simultaneous recordings directly from the left MPC and LPC in 3 human subjects using electrocorticography (ECoG; Figure 1A–B). Such rare recordings provide a unique opportunity to study neuronal population activity in the human brain with high spatiotemporal precision. We focused on subjects with electrode coverage over the left hemisphere given the strong neuroimaging evidence supporting lateralization of parietal activations during episodic retrieval (Hutchinson et al., 2009; Nelson et al., 2010). As part of a clinical evaluation for epilepsy surgery, subdural grid and strip electrode arrays were positioned over large areas of the MPC and LPC in each subject. Electrophysiological data from dual MPC/LPC implantations was recorded during task conditions that probed autobiographical episodic retrieval, and also during resting and sleeping states. In addition, resting state functional magnetic resonance imaging (rsfMRI) data was separately acquired from each subject to facilitate a direct quantitative comparison between electrophysiological and imaging measures of intrinsic coupling across parietal subregions.

Building upon a wide body of neuroimaging literature, we report novel information about the temporal dynamics of responses across MPC and LPC during episodic retrieval. We observed a zero time lag (delay) in the onset latency of activity between RSC/PCC and AG at the single trial level during retrieval. Furthermore, we found clear evidence for correlated electrophysiological activity between the same RSC/PCC and AG subregions during resting and sleeping states. Across the parietal lobe, intrinsic connectivity patterns strikingly recapitulated event-related task co-activation patterns and closely matched rsfMRI

connectivity in each subject. Collectively, our findings provide new information about the temporal engagement of human parietal subregions during episodic memory retrieval, and more generally, provide clear electrophysiological correlates of functional connectivity during resting and task states in the human cortex.

Results

Selective ECoG task responses in parietal subregions

Subjects performed a simple memory task previously shown to modulate ECoG (Dastjerdi et al., 2011; Foster et al., 2012) and fMRI (Kennedy and Courchesne, 2008) activity in the human parietal lobe (Figure 1C and S2, see Supplemental Experimental Procedures). Consistent with our previous work (Foster et al., 2012; Foster et al., 2013), ECoG data analyses focused on temporally resolved changes in high frequency broadband amplitude (HFB: 70–180 Hz, also known as high-gamma). HFB activity is an informationally rich and spatially precise measure of neuronal population response (Chang et al., 2010; Flinker et al., 2011; Miller, 2010), and importantly, is strongly correlated with blood oxygen level dependent (BOLD) fMRI (Hermes et al., 2012; Mukamel et al., 2005; Nir et al., 2007; Winawer et al., 2013), and population spiking activity in the local field potential (Manning et al., 2009; Mukamel et al., 2005; Nir et al., 2007; Ray and Maunsell, 2011). Therefore, the HFB spectral range provides a rich marker of local electrocortical activity of great translational utility between human and non-human primate research and more specifically between neuroimaging and electrophysiological data. As shown in Figure 1D-E, mean HFB amplitude responses across conditions differed between several parietal subregions, however the response profiles in RSC/PCC and AG were strikingly similar (see also Figure S1). Both RSC/PCC and AG displayed greater HFB responses to the “self-episodic” condition (e.g., “*I ate fruit yesterday*”), with progressively smaller mean HFB responses to the “self-semantic” (e.g., “*I eat fruit often*”), “self-judgment” (e.g., “*I am an honest person*”), and “other-judgment” (e.g., “*my neighbor is an honest person*”) conditions. In addition, both RSC/PCC and AG showed deactivation of HFB amplitude during a simple arithmetic “math” condition, consistent with our previous observations from the MPC (Foster et al., 2012).

Correlated ECoG task responses between RSC/PCC and AG

In light of the highly similar HFB response profiles of RSC/PCC and AG across all conditions, we sought to explore the correlation of HFB responses between parietal subregions at the single trial level. We compared the similarity of parietal subregion task responses by correlating the mean HFB amplitude across all trials for an entire experimental run (see Supplemental Experimental Procedures). Responses recorded simultaneously from the PCC and AG showed a strong positive correlation ($r = 0.83$, $p < 0.001$, $n = 178$, Figure 2), whereas comparing the same PCC seed to dorsal sites in the LPC revealed no significant correlation (Figure S3). These data suggest the presence of neuronal populations in specific locations of the MPC and LPC whose electrophysiological responses are tightly coupled and similarly modulated in magnitude, during both activation and deactivation, across different cognitive conditions.

To generalize this observation, we performed the same trial based correlation of HFB responses across all unique pairs of parietal electrodes in each subject, including both within (e.g., lateral-lateral = AG-SPL) and between (e.g., medial-lateral = PCC-SPL) surface comparisons. Therefore, we constructed a task correlation matrix for each subject based on trial-level mean HFB responses (Figure 3A, see Supplemental Experimental Procedures). Averaging correlations for each unique subregional pair across subjects revealed a consistent positive correlation between RSC/PCC and AG sites for repeated experimental runs (Figure 3B). A breakdown of RSC/PCC - AG task correlations suggested that these two parietal subregions were comodulated by all task conditions, with the strongest correlations being observed for the self-episodic and self-semantic conditions (Figure 3C). To ensure that overall task correlations were not driven by conditions with larger trial responses (e.g., self-episodic condition), task responses were normalized within condition (z-score) prior to correlation. This normalization procedure suggested a limited influence of response magnitudes, with normalized data and non-normalized data producing highly similar task correlation patterns (normalized vs. non-normalized similarity: S1 $r = 0.96$; S2 $r = 0.91$; S3 $r = 0.78$, all $p < 0.0001$).

Coordinated timing of ECoG task responses between RSC/PCC and AG

Given the strong trial based electrophysiological co-activation patterns between RSC/PCC and AG sites across subjects, we sought to further quantify the coordination of these responses with additional temporal precision. Specifically, we estimated the time of onset of HFB responses in RSC/PCC and AG sites at the single trial level. Our analyses focused on self-episodic trials given the consistency of maximal HFB responses to this condition and our specific interest in episodic retrieval. Using a robust method for estimating response onset latency (ROL, Figure S4), we obtained the HFB ROL values of each self-episodic trial for all RSC, PCC and AG sites (see Supplemental Experimental Procedures). For each site, the ROL was defined by the median ROL across trials (given the positive skew of ROL data). Interestingly, when comparing RSC/PCC and AG sites, we found no significant difference in the mean HFB ROL (mean, 95% ci: RSC/PCC = 674 ms, 555:820 ms; AG = 761 ms, 629:897 ms) for the self-episodic condition. The latency of HFB response onset in RSC/PCC and AG is consistent with our previous observations in the MPC in different experimental subjects under similar task conditions (mean MPC latency = 627 ms) (Foster et al., 2012). This similarity of ROL did not significantly differ for true or false responses in RSC/PCC (mean, 95% ci: true = 734 ms, 568:940 ms; false = 662 ms, 527:800 ms) or AG (mean, 95% ci: true = 764 ms, 624:936 ms; false = 791 ms, 647:1020 ms).

As mean ROL data suggested no significant difference in the response timing between RSC/PCC and AG during retrieval, we next compared differences in ROL at the single trial level (i.e., non-collapsed trial data) for all possible RSC/PCC-AG electrode pairs. Therefore, electrode sites were included in this analysis based solely on anatomical location to limit data selection bias, which included sites of differing response magnitude. Thus, for each unique RSC/PCC-AG electrode pair (n pairs = 68) we computed an ROL difference value (i.e., onset delay) for each trial by subtracting the ROL of a given RSC/PCC site from the ROL of a given AG site (see Supplemental Experimental Procedures). This difference value would therefore be positive if AG ROL precedes RSC/PCC and negative if RSC/PCC ROL

precedes AG. Also, in taking relative ROL differences for each trial, we account for natural variation in absolute ROL values across different stimuli. Strikingly, the distribution of ROL differences between RSC/PCC and AG across all subjects was strongly peaked around zero, displaying no skew or non-zero peaks, suggesting no dominant lag-lead difference (i.e., delay) in the time of response onsets of neuronal population responses between these regions (Figure 4A; delay median, 99% ci = 0 ms, −16:16 ms, n = 3,288). This distribution of ROL differences between RSC/PCC and AG was consistent across individual subjects (see Figure S5A). In addition, ROL differences were not significantly different for true (delay median, 99% ci = 0 ms, −22:32 ms, n = 1,010) or false (delay median, 99% ci = 2 ms, −16:23 ms, n = 2,278) response trials of the self-episodic condition.

As an active control within parietal cortex, we also compared the ROL differences between RSC/PCC sites and SPL sites responsive to the self-episodic condition (n pairs = 82; see Supplemental Experimental Procedures). In contrast to AG, ROL difference values between RSC/PCC and SPL displayed a rightward shifted and less peaked distribution, suggesting SPL is often engaged after RSC/PCC (Figure 4A; delay median, 99% ci = 505 ms, 459:543 ms, n = 3,886). Performing the same analysis for responsive IPS sites (n pairs = 72) provided a similarly right-shifted distribution, but centering earlier than the SPL (delay median, 99% ci = 154 ms, 119:181 ms, n = 3,457). Additionally, we performed further active controls using visual and motor sites outside of the parietal lobe in each subject that provided strong expectations for relative ROL timing (see Supplemental Experimental Procedures). As predicted, ROL differences between RSC/PCC sites and visual sites (n pairs = 45) showed a leftward shifted distribution with high kurtosis and positive skew (Figure 4A; delay median, 99% ci = −252 ms, −268: −231 ms, n = 2,319). This distribution indicates that the timing of visual HFB onsets were consistently prior to RSC/PCC sites with limited variation of ROL delay. Conversely, the distribution of HFB ROL differences between RSC/PCC sites and motor sites (n pairs = 67) showed a large rightward shift with less kurtosis (Figure 4A; delay median, 99% ci = 907 ms, 859:959 ms, n = 3,150). This distribution indicates that the timing of motor activity (typically reflecting a contra-lateral button press to respond *true* or *false*) was after the time of onset of visual, RSC/PCC, AG, IPS and SPL activations, and with a greater variation than visual sites (owing to the variation in reaction times for the task). The significance of these differences in ROL distributions across active control sites is clearly seen when comparing the probability density of each distribution (Figure 4B). Given the confidence intervals of distribution medians, each of the active control distributions (SPL, IPS, visual & motor) was significantly different from the distribution of AG ROL differences (confirmed with Wilcoxon rank test, Bonferroni corrected, all $p < 0.001$). Importantly, our observations of task correlation and temporal coordination between RSC/PCC and AG were also replicated when applying a more standard cross-correlation analysis to HFB task data (see Figure S6). Together, these findings suggest a tight minimal lag coupling of activation onset in the RSC/PCC and AG that closely follows the activation of early visual cortex and precedes the onset of activity in the dorsal IPS/SPL and motor cortex during episodic autobiographical retrieval (Figure 4C).

Correlated ECoG resting state activity between RSC/PCC and AG

Given the similarity of response magnitude and timing between RSC/PCC and AG during task conditions, we sought to quantify the degree of intrinsic coupling between these same subregions during the resting state. Based on a large body of evidence from human brain imaging, one would posit that large extents of the RSC/PCC and AG should display intrinsic functional connectivity given their shared membership in the DMN, which functionally dissociates these areas from other parietal subregions (Nelson et al., 2010). To approximate the timescale of BOLD activity observed for rsfMRI analyses, we extracted the slow (< 1 Hz) ongoing fluctuations of HFB amplitude from spontaneous resting state ECoG (rsECoG) data. This composition of frequency bands follows prior work suggesting that this range of activity best correlates with spontaneous BOLD data and yields the most consistent and anatomically specific spatial correlations (Keller et al., 2013; Leopold et al., 2003; Nir et al., 2008). Figure 5A–C depicts the basic processing steps to obtain the slow time varying HFB signal. Following classical rsfMRI methods, we performed a seed-based approach of correlating all unique electrode pairs between MPC and LPC for each subject. When a seed in the RSC/PCC was selected, correlations of slow HFB fluctuations were significantly and selectively localized to AG recording sites on the lateral surface (Figure 5D, see Supplemental Experimental Procedures). Using alternative frequency bands we observed a similar correlation pattern for the low beta range (13 – 29 Hz), but no similarity for the delta (0.5 – 3 Hz), theta (4 – 7 Hz), alpha (8 –12 Hz), high beta (30 – 39 Hz) or gamma (40 – 69 Hz) ranges (all focused on slow, < 1 Hz, fluctuations, Figure 5E) for the same seed region.

Across subjects, rsECoG analyses consistently showed strong positive correlations between the RSC/PCC and AG during the resting state (Figure 6). Furthermore, when selecting the same RSC/PCC seed regions within subjects and plotting the distribution of correlation values in LPC, we observed a strikingly similar spatial pattern of correlation for event related task data and spontaneous rest data (Figure 6A). In addition, this pattern, which is dominated by selective AG correlation, also showed a strong resemblance to the distribution of HFB amplitude increases in the LPC during the self-episodic condition (Figure 6B). Therefore, during episodic autobiographical retrieval, the spatial pattern of HFB responses appears highly similar to the spatial patterns of significant MPC-LPC correlations during both task and resting state conditions. Importantly, we note that task correlation data is derived from trial based activation changes in HFB amplitude whereas resting state correlations are based on slow (< 1 Hz) fluctuations of spontaneous HFB amplitude.

Similarity of ECoG parietal connectivity during task, rest and sleep states

While the correlation analysis of task and resting state was performed on highly different data sets and time-scales, it may be argued that the resting state data contains diluted levels of spontaneous recall processes of an autobiographical nature, which may explain the similar findings between states. A growing literature in functional neuroimaging has debated this issue (Buckner et al., 2008), with one important observation being that patterns of resting state connectivity are preserved during states of minimal cognition such as sedation (Greicius et al., 2008), anesthesia (Martuzzi et al., 2010) and sleep (Samann et al., 2011). Following this approach, we obtained ECoG data from each subject during nocturnal sleep (Figure S7) and performed the same resting state analysis. As shown in Figure 6A, using the

same MPC seed locations as in the rest and task data, a highly similar pattern of correlation centered on the AG was observed during sleep across subjects (Ramot et al., 2013).

To broaden our analysis, we performed a direct comparison of all MPC-LPC pairs for each subject across task, rest and sleep states. For this we obtained a correlation matrix of the same dimension for each state (i.e., task, rest and sleep), as shown in Figure 6C for an example subject (S3). We then directly tested the degree of similarity between these matrices using permutation matrix correlation (Mantel's test, see Supplemental Experimental Procedures). Initially, we limited our matrix comparison to only unique MPC-LPC pairs and excluded within-MPC or within-LPC pairs to limit the possible bias of trivial correlations for proximal sites (i.e., correlations between neighboring electrodes). However, performing a full matrix comparison (i.e., all pairs) did not substantially change the between-state similarity estimates (see Figure S8B). Figure 6D shows the scatter plots and correlation values for the three state comparisons of example subject S3. Across states, there is a robust positive correlation between connectivity matrices. As can be seen in Figure 6E, the high similarity of parietal subregion connectivity between states was consistent and strongly significant for each subject ($p < 0.01$). Figure 6E also indicates that the greatest similarity between states was for the rest versus sleep comparison. Apart from the gamma band range, other frequency bands did not display significant connectivity similarity across states (see Figure S8).

Similarity of parietal resting state connectivity between ECoG and fMRI

Our data suggest electrophysiological activity in human parietal cortex may contain highly correlated spatial patters of intrinsic fluctuations that closely resemble those observed with rsfMRI. To directly support this claim, we obtained rsfMRI from each subject and quantified the similarity between ECoG and fMRI resting state data. To facilitate this comparison, we extracted the BOLD time course from regions of interest (ROI) within parietal cortex defined by the location of ECoG electrodes in each subject. Figure 7A,B shows a qualitative comparison of the overlap between rsECoG and rsfMRI in an example subject (S3). As detailed above, when examining a seed in the MPC, rsECoG data display a selective and highly significant positive correlation with sites in the AG (Figure 7A). When using the same seed location for rsfMRI analysis, we also observed a strikingly similar pattern of positive correlation with the AG, which closely overlaps with significantly correlated ECoG sites and other nodes of the DMN (Figure 7B). Matching analyses performed above, we quantified the similarity of connectivity (i.e., correlation matrices) for all unique parietal subregion pairs between rsECoG and rsfMRI. Figure 7C shows that rsECoG and rsfMRI data were significantly correlated in each subject ($p < 0.01$, Mantel's test).

Given the similarity between ECoG and fMRI resting state data, we explored the degree to which electrophysiological measures conform to regional and network parcellations of cerebral cortex as commonly estimated with fMRI. As an initial step in this direction, Figure 8 shows an example comparison between rsECoG and rsfMRI data where correlation profiles were compared for seed regions traversing the inferior parietal lobule from the SMG to AG. This simple approach to boundary identification directly follows a technique previously described by Cohen et al. (2008) and more recently by Wig et al. (2014). Local

correlations for both ECoG and fMRI data displayed a clear transitional change between SMG and AG, with a concurrent increase in correlation strength with the distal PCC seed region for LPC seeds closer to AG, a finding consistent with the imaging reports (Cohen et al., 2008; Wig et al., 2014).

Discussion

Simultaneous measurements of electrophysiological activity from large areas of the left medial and lateral parietal cortices in human subjects revealed localized neuronal population responses, as indexed by HFB amplitude, within the RSC/PCC (medial) and AG (lateral) during conditions of episodic retrieval. RSC/PCC and AG displayed a similar profile of mean HFB response across all task conditions, which reflected a strong positive correlation of single trial responses between these subregions. Further analyses demonstrated that the relative timing of HFB response onset between RSC/PCC and AG was simultaneous during autobiographical retrieval. In addition, we explored the spatial organization of intrinsic dynamics across parietal cortex during rest and sleep states, focusing on correlated patterns of slow (< 1 Hz) HFB activity. Strikingly, we observed highly similar electrophysiological patterns of connectivity across task, rest and sleep states, in each subject. Finally, intrinsic electrophysiological connectivity patterns were shown to highly correlate with rsfMRI connectivity data extracted from matching recording locations within each subject.

Parietal cortex dynamics during episodic retrieval

Our observations are consistent with neuroimaging findings of left parietal activations during episodic memory retrieval (Cabeza et al., 2008; Wagner et al., 2005), and importantly provide additional temporal information about these activation patterns. Neuroimaging studies have consistently shown that cued retrieval of autobiographical events engages the RSC/PCC and AG, along with other nodes of the DMN (Spreng et al., 2009). Similarly, for tasks of recognition memory, activation of RSC/PCC and AG is particularly enhanced when recollecting item source information (i.e., specific item details) (Cabeza et al., 2008; Wagner et al., 2005). This ‘old/new’ source memory effect is observed for both lateral and medial parietal regions, with a robust left hemisphere dominance (Hutchinson et al., 2009). While our current findings support left hemisphere parietal retrieval effects, our previous ECoG work has shown similar RSC/PCC responses also in the right hemisphere (Foster et al., 2012). This work employed highly similar experimental and data analysis methods to the current study, supporting a comparison between data sets. Therefore, the observation of bilateral MPC responses raises an important question of how lateral and medial parietal subregions differ in their response lateralization during episodic retrieval.

In comparing response timing in MPC and LPC, we observed no consistent difference in the latency of HFB response onset between the RSC/PCC and AG during episodic retrieval. A zero-lag delay of response onset between two regions is indicative of a mediator node that would initially provide simultaneous inputs, separately engaging both of these regions. Natural candidates for this mediator would be MTL structures with anatomical projections to MPC and LPC subregions either directly or through the thalamus. Tracing studies in non-human primates suggest reciprocal connections of RSC/PCC and AG with MTL structures

and thalamic nuclei (Buckwalter et al., 2008; Kobayashi and Amaral, 2003, 2007; Parvizi et al., 2006). The putative role of the MTL as a common mediator is also supported by our own previous findings. Using simultaneous intracranial recordings from the human RSC/PCC and MTL cortices, we observed selective transient phase synchrony in the theta band range (3 – 5 Hz) between the human RSC and MTL during the same autobiographical retrieval task conditions employed here (Foster et al., 2013). We observed that phase synchrony between the RSC and MTL consistently occurred prior to the local activation (i.e., increased HFB amplitude) of the RSC, a temporal sequence consistent with RSC/PCC and AG ROL reported here. Alternatively, the temporal co-activation of RSC/PCC and AG may reflect a shared activation threshold, such that small delays of input activity are integrated to a common activation boundary (Fisch et al., 2009).

Based on the shared onset of activation in RSC/PCC and AG sites, one may hypothesize a degree of independence between these two regions such that initial functional engagement of one region does not rely on the outputs of computations performed in the other. Therefore, RSC/PCC and AG may operate in parallel, focusing on different features of retrieval outputs from the MTL. Importantly, we note that while the onset of activity in RSC/PCC and AG may be mediated by the MTL, post-onset correlation between these two regions, along with their resting state coupling, is likely to be supported by their direct reciprocal connectivity. Deciphering the unique functional roles of RSC/PCC and AG during retrieval will require future targeted experiments to manipulate various features of episodic retrieval content.

Neurophysiological correlates of intrinsic connectivity

Consistent with the above discussion, prior fMRI based network analysis of the DMN has identified the RSC/PCC and AG, together with structures in the MTL, as a dissociable sub-network (Andrews-Hanna et al., 2010) of this system. Our findings suggest highly similar patterns of parietal connectivity can be observed with direct measures of neuronal population activity. Importantly, our findings are strengthened by the use of multisite grid recordings in each subject, sampling a large mantel of the parietal cortex. For example, despite recording from multiple regions in the LPC, we observed slow fluctuations of HFB activity to consistently and specifically correlate between neuronal populations within the RSC/PCC and AG. The anatomical selectivity of this correlation is particularly striking given the long-range distance between the medial and lateral surface, suggesting that these correlations are not due to volume conduction effects. By comparison, slow fluctuations of other canonical frequency bands either failed to reveal significant functional connectivity or revealed significant correlations across much of the LPC with less anatomical selectivity (Figure 5E). Only slow fluctuations of low beta activity (13–29 Hz) were similar to the HFB range, which is consistent with prior observations (Hipp et al., 2012). Therefore, it is important to define electrophysiological correlates not only by the strength of inter-regional connectivity, but also by spatial selectivity (i.e., correspondence with known functional-anatomical boundaries).

While the biophysical origins and spectral properties of HFB activity are still being elucidated, one mechanism of generating this signal is via the dendritic filtering of incoming

synaptic potentials (Einevoll et al., 2013; Miller, 2010), which is associated with a strong metabolic drive precipitating the BOLD signal (Logothetis and Wandell, 2004). Together, the temporal, spatial and biophysical properties of HFB activity support the hypothesis that this signal may provide a robust correlate of fMRI resting state connectivity (Keller et al., 2013).

Correspondence of intrinsic and task connectivity

The similarity of intrinsic and task evoked connectivity patterns points to important organizational features of large-scale brain systems and may provide an assay of macro-scale brain network integrity. While such questions were beyond the scope of the present study, our data strongly support the observation that intrinsic correlation patterns, captured by slow spontaneous HFB fluctuations, recapitulate network activation patterns observed during task conditions (Cole et al., 2014; Ramot et al., 2013; Smith et al., 2009). For example, Ramot et al. (2013) recently reported that fluctuations of high-frequency activity during slow-wave sleep recapitulated the mean spatial patterns of high-frequency activity observed during task conditions in human sensory cortex. This similarity between states promotes the importance of understanding how spontaneous neural dynamics could influence the configuration of functional brain states. One compelling hypothesis posits that spontaneous activity patterns reflect the organization and strength of network connections, as influenced by the recent statistical history of activation patterns (Harmelech and Malach, 2013). From this view, spontaneous activity may provide insight into the topological organization of brain networks/circuits, and their functional repertoires (Luczak et al., 2009).

In conclusion, we wish to emphasize that the goal of the present study was to quantify the electrophysiological interactions between neuronal populations of the medial and lateral parietal nodes of the human DMN during task conditions, as well as resting and sleeping states. By comparing these data with rsfMRI in the same subjects, we aimed to identify clear electrophysiological correlates of DMN connectivity. We are mindful that future investigations employing different experimental designs are needed to decipher the electrophysiological correlates of specific types of mnemonic processes in the human parietal lobe. Additional experiments are also needed to dissociate the differential role(s) of medial and lateral parietal subregions during memory retrieval. Lastly, our current data are from a specific brain network (i.e., DMN), and future studies are needed to determine if the electrophysiological signature of functional connectivity that we report is generalizable across other large-scale human brain networks.

Experimental Procedures

Subjects

Intracranial recordings reported in the present study were obtained from three human subjects at the Laboratory of Behavioral and Cognitive Neurology in the Stanford University Medical Center (California, USA). Subjects were aged 39, 36 and 22 (years, m ± std = 32.3 ± 9), with the gender of male, female and female, respectively (S1–3). Each subject was implanted with subdural intracranial electrodes over the left cerebral hemisphere as part of their evaluation for the neurosurgical treatment of refractory epilepsy (Nair et al., 2008).

Clinically, seizure onset foci were identified as left insula (S1), left medial primary motor cortex (S2) and left supplementary motor cortex (S3), respectively. All subjects were identified as right-handed and spoke English as a first language. Prior to any experimentation, all subjects provided verbal and written consent to participate in the research presented here, which was approved by the Stanford Institutional Review Board.

Electrode implantation

Subjects were implanted intracranially with grid and strip configuration subdural platinum electrodes (Adtech Medical Instruments) for the purpose of clinical monitoring. All electrodes were 4 mm in diameter and imbedded in a flexible silicon sheet, with each electrode having an exposed (recording) diameter of 2.3 mm. For the majority of implanted electrodes, inter-electrode spacing was 10 mm (center to center). For S2 and S3, some strip electrodes had a higher density inter-electrode spacing of 5 mm (center to center). Importantly, all implantations were guided fully by clinical requirements and no implantation was performed for research purposes.

Intracranial electrodes were localized on the cortical surface using a fusion of pre- and post-operative imaging as previously described (Foster et al., 2012). Once the cortical location of electrodes was obtained for each subject, we identified all electrodes falling within the medial and lateral parietal cortex and classified them into parietal subregions (using surface projections and 3D images) (see Figure 1 and Supplemental Experimental Procedures).

Electrophysiological recording

All electrophysiological data presented were obtained from subdural electrocorticography (ECoG) recordings. ECoG data was acquired with a band pass filter of 0.5–300 Hz and a sampling rate of 3,052 Hz, via a multichannel research system (Tucker Davis Technologies). For recording, ECoG signals were referenced to the most electrographically silent channel outside of the identified seizure zone, and later re-referenced for data analysis. For nocturnal sleep recordings, we obtained ECoG data recorded by a clinical monitoring system (Nihon Kohden). These data were recorded using the same reference montage, but with different sample rates (S1 = 1000 Hz; S2 = 1000 Hz; S3 = 500 Hz).

Experimental task - ECoG

All experimental task recordings were performed at the bedside in the subject's private clinical suite. To perform the task, subjects were asked to provide true or false judgments for five different stimulus types that were visually presented on a laptop computer (Apple MacBook Pro). This task was previously employed to effectively probe the electrophysiology of the human default mode network (DMN) (Dastjerdi et al., 2011; Foster et al., 2012; Foster et al., 2013) (see Figure 1 and Supplemental Experimental Procedures).

Resting state - ECoG

Two types of resting state data are reported. Firstly, standard passive resting state data was recorded during continuous periods of eyes closed rest. Secondly, spontaneous data was also recorded during periods of nocturnal sleep in each subject. As research recordings were not continuous over a 24-hour period, sleep data was obtained from continuous clinical

recordings as noted above. Sleep data for each subject reflects periods of stage 2/3 nocturnal sleep as shown in Figure S7. Full polysomnography for sleep staging was not recorded. While recorded resting state data differed in duration, all reported analyses were performed on truncated 4 min duration data segments.

Resting state - fMRI

Resting state fMRI data reported here were obtained at the Center for Cognitive and Neurobiological Imaging (S2–3), and the Richard M. Lucas Center for Imaging at Stanford University (S1). Scanning was performed pre-operatively in S1–2, and postoperatively for S3 due to clinical factors. For S2–3, resting-state EPI sequence scans were acquired on a 3T GE scanner (30 slices, 4.0 mm isotropic voxels, TR = 2000 ms, FOV = 100 mm, TE = 30 ms, flip angle = 77 deg, bandwidth = 127.68 kHz) with a 32-channel head coil (duration = 8 minutes and 10 minute respectively). For S1, resting-state spiral sequence scans were obtained on a 3T GE scanner (30 slices, 4.0 mm isotropic voxels, TR=2000 ms, FOV= 220 mm, TE = 30 ms, flip angle = 77 deg, bandwidth = 127.68 kHz) with a 32-channel head coil (duration = 6 minutes).

Data processing - ECoG

All experimental task and resting state ECoG data were processed off-line using custom routines programed in MATLAB (MathWorks). Prior to data processing, all channels clinically identified within the ictogenic zone or those electrodes observed as corrupted during recording were excluded from all data analysis. All data preprocessing was performed at the single subject/single electrode level. For each subject, all non-excluded electrodes were notch filtered to remove 60 Hz interference as well as its harmonics. Notch filtered data was then re-referenced to the common average in each subject. After re-referencing, each electrode was automatically inspected for outliers, defined as voltage values >5 standard deviations from the electrode mean voltage, with outlier data points logged for subsequent analyses. The notch filtered, re-referenced data was then used for all subsequent data analysis.

High Frequency Broadband (HFB) Amplitude

High frequency broadband (HFB) amplitude, defined by a 70–180 Hz band pass range in the present study, was used throughout all analyses as the key electrophysiological marker of electrocortical activity (Miller et al., 2014). Frequency normalized HFB power was estimated using the following steps: i) the raw time series (notch filtered, re-referenced) was down sampled to 436 Hz and then filtered between 70–180 Hz using sequential band pass windows of 10 Hz (i.e. 70–80, 80–90, 90–100 …170–180), via a two-way zero-phase lag FIR filter. ii) the amplitude (envelope) of each narrow band signal was then calculated by taking the modulus of the analytic signal obtained from a Hilbert transform. iii) each narrow band amplitude time series was then normalized to its own mean amplitude, expressed as a percentage of the mean. iv) finally, each of the normalized narrow band amplitude time series was averaged together, producing a single amplitude time series for each channel. These processing steps aim to normalize (flatten) the power across frequencies within the broad 70–180 Hz range, partially correcting for the 1/frequency decay of power in the spectrum that enhances lower frequency components.

HFB response and latency

To quantify event-related HFB responses, we epoched trials for each condition locked to stimulus onset (−200 ms pre-stimulus to 2000 ms post-stimulus). Trials were then averaged for all epoch time points to obtain the mean HFB response for each condition. To obtain a singular HFB response value across conditions for each electrode, we averaged the mean HFB response within a 400–900 ms post-stimulus window. This window was chosen because we predicted late onset activity in parietal cortex to the employed task (Foster et al., 2012), which would exclude early non-selective activity to the visual stimulus and late response-locked (i.e. motor) activity. In order to characterize the latency of activation across electrodes for the self-episodic condition, we estimated the HFB response onset latency (ROL), using a modified version of a previously described technique (Foster et al., 2012) (see Figure S4 and Supplemental Experimental Procedures).

Slow HFB fluctuation

Analysis of resting state ECoG data focused on slow spontaneous fluctuations in HFB amplitude (Foster and Parvizi, 2012). To obtain this signal, the continuous HFB amplitude was estimated as described above and then low pass filtered at 1 Hz, using a 4^{th} order two-way zero phase lag Butterworth filter. This slow time-varying HFB amplitude signal (i.e. HFB amplitude fluctuations below 1 Hz) was then used for all resting state correlation analyses, following previous investigators (Keller et al., 2013; Nir et al., 2008).

Data processing – fMRI

Resting-state fMRI (rsfMRI) data were processed and analyzed using the FMRIB Software Library (FSL: v5.0.6). Raw functional data were processed by applying motion correction, removal of non-brain structures, and spatial smoothing with a 6mm FWHM Gaussian kernel. Processed functional data were then aligned to the subject's high-resolution T1-weighted image, which was subsequently registered to the MNI152 standard space image via affine linear registration. Registered data were corrected via noise regression of movement, cerebral spinal fluid, white matter, and global signal. Finally, the data were additionally filtered with a band pass range of 0.01 – 0.10 Hz.

Regions of interest (ROI) corresponding to electrode locations in each subject were created by first constructing a 5 mm radius sphere at each electrode coordinate. To limit these ROI to cortical tissue, a gray matter mask (based on cortical segmentation) was applied to each ROI. These masked ROI were then transformed to the same standard space as the functional data, and the mean rsfMRI time series across volumes was extracted for each ROI. Prior to correlation analysis, each time series had the mean value subtracted and was then detrended (linear least squares fit).

Connectivity analyses – ECoG & fMRI

Connectivity analyses focused on correlated HFB (ECoG) and BOLD (fMRI) activity. For all data, correlation values were estimated via Pearson's correlation coefficient (r) between all sites (electrodes or ROIs), producing a correlation matrix for each data set. We tested the similarity of correlation matrices across states (i.e. task, rest and sleep) and modalities (ECoG and fMRI) using Mantel's test (Mantel, 1967) of matrix similarity. This procedure

performs a randomization test of correlation between two matrices, where iterative permutation of one matrix is used to construct a null distribution of matrix similarity (correlation). We performed Mantel's test using 1000 permutations to estimate the p-value of each matrix similarity comparison. To satisfy test assumptions, matrix data (r-values) were first normalized using a Fisher-z transform, and scatter plots were inspected for heteroscedasticity and outliers.

Supplementary Material

Refer to Web version on PubMed Central for supplementary material.

Acknowledgments

The authors thank Anthony Wagner, Bernhard Staresina, Jessica Schrouff, Jonas Richiardi and Michael Waskom for useful feedback on data analysis and visualization. This work was supported by research grants from the Stanford NeuroVentures Program, US National Institute of Neurological Disorders and Stroke (R01NS078396) and US National Science Foundation (BCS1358907) to J.P, and by a career development award from the US National Institute of Mental Health (K99MH103479) to B.L.F.

References

Andrews-Hanna JR, Reidler JS, Sepulcre J, Poulin R, Buckner RL. Functional-anatomic fractionation of the brain's default network. Neuron. 2010; 65:550–562. [PubMed: 20188659]

Buckner RL, Andrews-Hanna JR, Schacter DL. The brain's default network: anatomy, function, and relevance to disease. Ann N Y Acad Sci. 2008; 1124:1–38. [PubMed: 18400922]

Buckwalter JA, Parvizi J, Morecraft RJ, van Hoesen GW. Thalamic projections to the posteromedial cortex in the macaque. J Comp Neurol. 2008; 507:1709–1733. [PubMed: 18253938]

Cabeza R, Ciaramelli E, Olson IR, Moscovitch M. The parietal cortex and episodic memory: an attentional account. Nat Rev Neurosci. 2008; 9:613–625. [PubMed: 18641668]

Chang EF, Rieger JW, Johnson K, Berger MS, Barbaro NM, Knight RT. Categorical speech representation in human superior temporal gyrus. Nat Neurosci. 2010; 13:1428–1432. [PubMed: 20890293]

Cohen AL, Fair DA, Dosenbach NU, Miezin FM, Dierker D, Van Essen DC, Schlaggar BL, Petersen SE. Defining functional areas in individual human brains using resting functional connectivity MRI. Neuroimage. 2008; 41:45–57. [PubMed: 18367410]

Cole MW, Bassett DS, Power JD, Braver TS, Petersen SE. Intrinsic and task-evoked network architectures of the human brain. Neuron. 2014; 83:238–251. [PubMed: 24991964]

Dastjerdi M, Foster BL, Nasrullah S, Rauschecker AM, Dougherty RF, Townsend JD, Chang C, Greicius MD, Menon V, Kennedy DP, Parvizi J. Differential electrophysiological response during rest, self-referential, and non-self-referential tasks in human posteromedial cortex. Proc Natl Acad Sci U S A. 2011; 108:3023–3028. [PubMed: 21282630]

Einevoll GT, Kayser C, Logothetis NK, Panzeri S. Modelling and analysis of local field potentials for studying the function of cortical circuits. Nat Rev Neurosci. 2013; 14:770–785. [PubMed: 24135696]

Fisch L, Privman E, Ramot M, Harel M, Nir Y, Kipervasser S, Andelman F, Neufeld MY, Kramer U, Fried I, Malach R. Neural "ignition": enhanced activation linked to perceptual awareness in human ventral stream visual cortex. Neuron. 2009; 64:562–574. [PubMed: 19945397]

Flinker A, Chang EF, Barbaro NM, Berger MS, Knight RT. Sub-centimeter language organization in the human temporal lobe. Brain Lang. 2011; 117:103–109. [PubMed: 20961611]

Foster BL, Dastjerdi M, Parvizi J. Neural populations in human posteromedial cortex display opposing responses during memory and numerical processing. Proc Natl Acad Sci U S A. 2012; 109:15514–15519. [PubMed: 22949666]

Foster BL, Kaveh A, Dastjerdi M, Miller KJ, Parvizi J. Human retrosplenial cortex displays transient theta phase locking with medial temporal cortex prior to activation during autobiographical memory retrieval. J Neurosci. 2013; 33:10439–10446. [PubMed: 23785155]

Foster BL, Parvizi J. Resting oscillations and cross-frequency coupling in the human posteromedial cortex. Neuroimage. 2012; 60:384–391. [PubMed: 22227048]

Greicius MD, Kiviniemi V, Tervonen O, Vainionpaa V, Alahuhta S, Reiss AL, Menon V. Persistent default-mode network connectivity during light sedation. Hum Brain Mapp. 2008; 29:839–847. [PubMed: 18219620]

Greicius MD, Krasnow B, Reiss AL, Menon V. Functional connectivity in the resting brain: a network analysis of the default mode hypothesis. Proc Natl Acad Sci U S A. 2003; 100:253–258. [PubMed: 12506194]

Harmelech T, Malach R. Neurocognitive biases and the patterns of spontaneous correlations in the human cortex. Trends Cogn Sci. 2013; 17:606–615. [PubMed: 24182697]

Hermes D, Miller KJ, Vansteensel MJ, Aarnoutse EJ, Leijten FS, Ramsey NF. Neurophysiologic correlates of fMRI in human motor cortex. Hum Brain Mapp. 2012; 33:1689–1699. [PubMed: 21692146]

Hipp JF, Hawellek DJ, Corbetta M, Siegel M, Engel AK. Large-scale cortical correlation structure of spontaneous oscillatory activity. Nat Neurosci. 2012; 15:884–890. [PubMed: 22561454]

Hutchinson JB, Uncapher MR, Wagner AD. Posterior parietal cortex and episodic retrieval: convergent and divergent effects of attention and memory. Learn Mem. 2009; 16:343–356. [PubMed: 19470649]

Keller CJ, Bickel S, Honey CJ, Groppe DM, Entz L, Craddock RC, Lado FA, Kelly C, Milham M, Mehta AD. Neurophysiological investigation of spontaneous correlated and anticorrelated fluctuations of the BOLD signal. J Neurosci. 2013; 33:6333–6342. [PubMed: 23575832]

Kennedy DP, Courchesne E. Functional abnormalities of the default network during self- and other-reflection in autism. Soc Cogn Affect Neurosci. 2008; 3:177–190. [PubMed: 19015108]

Kobayashi Y, Amaral DG. Macaque monkey retrosplenial cortex: II. Cortical afferents. J Comp Neurol. 2003; 466:48–79. [PubMed: 14515240]

Kobayashi Y, Amaral DG. Macaque monkey retrosplenial cortex: III. Cortical efferents. J Comp Neurol. 2007; 502:810–833. [PubMed: 17436282]

Leopold DA, Murayama Y, Logothetis NK. Very slow activity fluctuations in monkey visual cortex: implications for functional brain imaging. Cereb Cortex. 2003; 13:422–433. [PubMed: 12631571]

Logothetis NK, Wandell BA. Interpreting the BOLD signal. Annu Rev Physiol. 2004; 66:735–769. [PubMed: 14977420]

Luczak A, Bartho P, Harris KD. Spontaneous events outline the realm of possible sensory responses in neocortical populations. Neuron. 2009; 62:413–425. [PubMed: 19447096]

Manning JR, Jacobs J, Fried I, Kahana MJ. Broadband shifts in local field potential power spectra are correlated with single-neuron spiking in humans. J Neurosci. 2009; 29:13613–13620. [PubMed: 19864573]

Mantel N. The detection of disease clustering and a generalized regression approach. Cancer Res. 1967; 27:209–220. [PubMed: 6018555]

Martuzzi R, Ramani R, Qiu M, Rajeevan N, Constable RT. Functional connectivity and alterations in baseline brain state in humans. Neuroimage. 2010; 49:823–834. [PubMed: 19631277]

Miller KJ. Broadband spectral change: evidence for a macroscale correlate of population firing rate? J Neurosci. 2010; 30:6477–6479. [PubMed: 20463210]

Miller KJ, Honey CJ, Hermes D, Rao RP, denNijs M, Ojemann JG. Broadband changes in the cortical surface potential track activation of functionally diverse neuronal populations. Neuroimage. 2014; 85(Pt 2):711–720. [PubMed: 24018305]

Mukamel R, Gelbard H, Arieli A, Hasson U, Fried I, Malach R. Coupling between neuronal firing, field potentials, and FMRI in human auditory cortex. Science. 2005; 309:951–954. [PubMed: 16081741]

Nair DR, Burgess R, McIntyre CC, Luders H. Chronic subdural electrodes in the management of epilepsy. Clin Neurophysiol. 2008; 119:11–28. [PubMed: 18035590]

Nelson SM, Cohen AL, Power JD, Wig GS, Miezin FM, Wheeler ME, Velanova K, Donaldson DI, Phillips JS, Schlaggar BL, Petersen SE. A parcellation scheme for human left lateral parietal cortex. Neuron. 2010; 67:156–170. [PubMed: 20624599]

Nir Y, Fisch L, Mukamel R, Gelbard-Sagiv H, Arieli A, Fried I, Malach R. Coupling between neuronal firing rate, gamma LFP, and BOLD fMRI is related to interneuronal correlations. Curr Biol. 2007; 17:1275–1285. [PubMed: 17686438]

Nir Y, Mukamel R, Dinstein I, Privman E, Harel M, Fisch L, Gelbard-Sagiv H, Kipervasser S, Andelman F, Neufeld MY, et al. Interhemispheric correlations of slow spontaneous neuronal fluctuations revealed in human sensory cortex. Nat Neurosci. 2008; 11:1100–1108. [PubMed: 19160509]

Parvizi J, Van Hoesen GW, Buckwalter J, Damasio A. Neural connections of the posteromedial cortex in the macaque. Proc Natl Acad Sci U S A. 2006; 103:1563–1568. [PubMed: 16432221]

Raichle ME, MacLeod AM, Snyder AZ, Powers WJ, Gusnard DA, Shulman GL. A default mode of brain function. Proc Natl Acad Sci U S A. 2001; 98:676–682. [PubMed: 11209064]

Ramot M, Fisch L, Davidesco I, Harel M, Kipervasser S, Andelman F, Neufeld MY, Kramer U, Fried I, Malach R. Emergence of sensory patterns during sleep highlights differential dynamics of REM and non-REM sleep stages. J Neurosci. 2013; 33:14715–14728. [PubMed: 24027272]

Ray S, Maunsell JH. Different origins of gamma rhythm and high-gamma activity in macaque visual cortex. PLoS Biol. 2011; 9:e1000610. [PubMed: 21532743]

Samann PG, Wehrle R, Hoehn D, Spoormaker VI, Peters H, Tully C, Holsboer F, Czisch M. Development of the brain's default mode network from wakefulness to slow wave sleep. Cereb Cortex. 2011; 21:2082–2093. [PubMed: 21330468]

Smith SM, Fox PT, Miller KL, Glahn DC, Fox PM, Mackay CE, Filippini N, Watkins KE, Toro R, Laird AR, Beckmann CF. Correspondence of the brain's functional architecture during activation and rest. Proc Natl Acad Sci U S A. 2009; 106:13040–13045. [PubMed: 19620724]

Spreng RN, Mar RA, Kim AS. The common neural basis of autobiographical memory, prospection, navigation, theory of mind, and the default mode: a quantitative meta-analysis. J Cogn Neurosci. 2009; 21:489–510. [PubMed: 18510452]

Vilberg KL, Rugg MD. Memory retrieval and the parietal cortex: a review of evidence from a dual-process perspective. Neuropsychologia. 2008; 46:1787–1799. [PubMed: 18343462]

Vincent JL, Patel GH, Fox MD, Snyder AZ, Baker JT, Van Essen DC, Zempel JM, Snyder LH, Corbetta M, Raichle ME. Intrinsic functional architecture in the anaesthetized monkey brain. Nature. 2007; 447:83–86. [PubMed: 17476267]

Vincent JL, Snyder AZ, Fox MD, Shannon BJ, Andrews JR, Raichle ME, Buckner RL. Coherent spontaneous activity identifies a hippocampal-parietal memory network. J Neurophysiol. 2006; 96:3517–3531. [PubMed: 16899645]

Wagner AD, Shannon BJ, Kahn I, Buckner RL. Parietal lobe contributions to episodic memory retrieval. Trends Cogn Sci. 2005; 9:445–453. [PubMed: 16054861]

Wig GS, Laumann TO, Cohen AL, Power JD, Nelson SM, Glasser MF, Miezin FM, Snyder AZ, Schlaggar BL, Petersen SE. Parcellating an Individual Subject's Cortical and Subcortical Brain Structures Using Snowball Sampling of Resting-State Correlations. Cereb Cortex. 2014; 24:2036–2054. [PubMed: 23476025]

Winawer J, Kay KN, Foster BL, Rauschecker AM, Parvizi J, Wandell BA. Asynchronous broadband signals are the principal source of the BOLD response in human visual cortex. Curr Biol. 2013; 23:1145–1153. [PubMed: 23770184]

Highlights

- Human electrocorticography reveals default network regions in parietal cortex
- These parietal subregions regions display simultaneous response onset timing
- Parietal connectivity patterns are similar for task, rest and sleep states
- Parietal connectivity patterns are similar for electrophysiology and fMRI

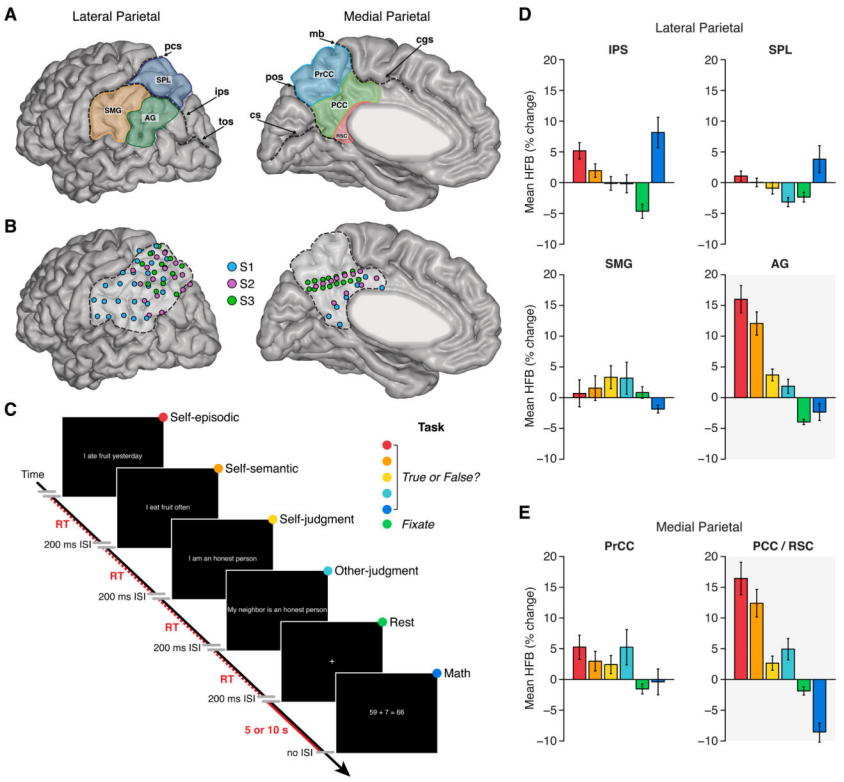

Figure 1. Parietal subregions, electrode locations, experimental task and task responses

A) Lateral and medial parietal lobe was divided into seven putative subregions. Lateral subregions were: supramarginal gyrus (SMG), angular gyrus (AG), intraparietal sulcus (IPS) and superior parietal lobule (SPL). Medial subregions were: precuneus cortex (PrCC), posterior cingulate cortex (PCC) and retrosplenial cortex (RSC). For group analyses, we combined PCC and RSC recording sites (RSC/PCC; see Supplemental Experimental Procedures). Sulci shown are: post-central sulcus (pcs), intra-parietal sulcus (ips), transverse occipital sulcus (tos), marginal branch (mg), cingulate sulcus (cgs), parieto-occipital sulcus (pos) and calcarine sulcus (cs). B) Lateral and medial views of electrode locations in left parietal cortex for all subjects normalized to a common brain (MNI). Highlighted boundaries demarcate left lateral and medial posterior parietal cortex. C) Subjects performed a simple task requiring true/false judgments of visually presented statements or equations as previously employed (Foster et al., 2012). Bar graphs show mean HFB response (with standard error of mean) across conditions for each parietal region of interest (D = lateral; E = medial) across all subjects. While dorsal parietal regions (IPS and SPL) display some similarity, most striking is the similar profile of HFB response between RSC/PCC and AG across conditions. See also Figures S1 and S2.

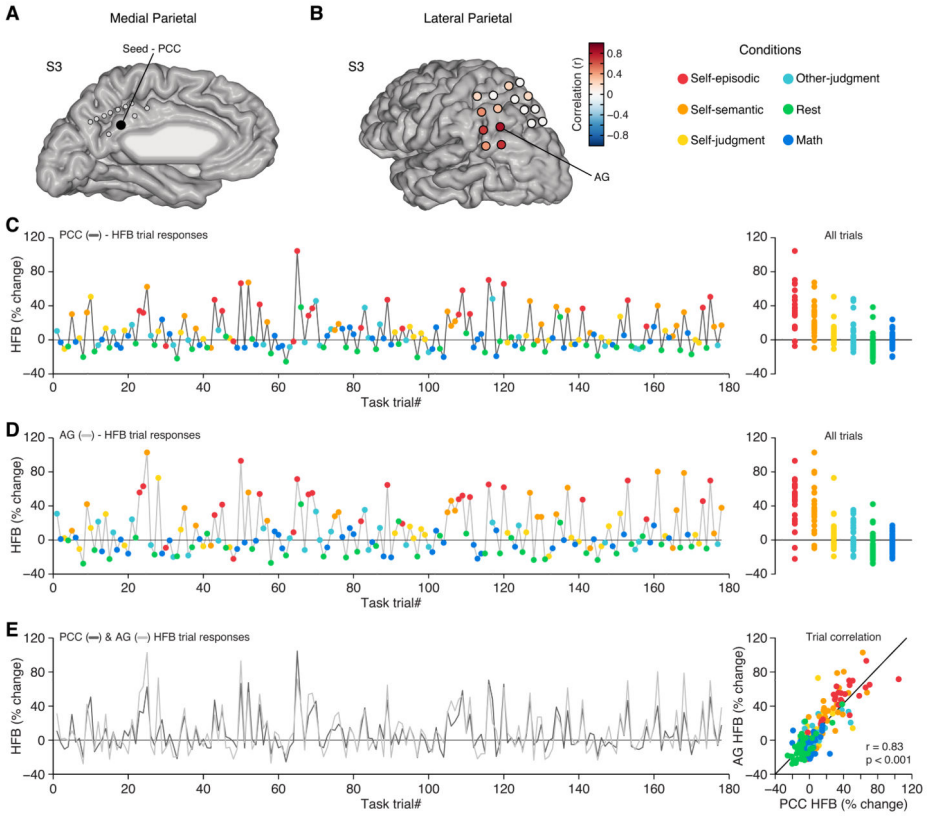

Figure 2. Correlated HFB trial responses between PCC and AG

A) Medial view of electrode sites for S3, with a PCC seed electrode highlighted. B) Lateral view of electrode sites in S3, where color indicates the correlation value of task responses with respect to the PCC seed electrode in (A). C) HFB responses for all trials (n = 178) across a single experimental run for the PCC electrode in (A). Each trial response reflects the mean HFB response for the time window 400–900 ms post-stimulus presentation. Right panel shows all trials for each condition, recapitulating the response profile of group data in Figure 1. D) Single trial HFB responses for the AG electrode in (B) from the same experimental data as in (C). E) Time series of trial responses from (C) and (D) reflecting PCC and AG respectively, display a strong positive correlation. Scatter plot displays all trial responses for PCC versus AG. See also Figure S3.

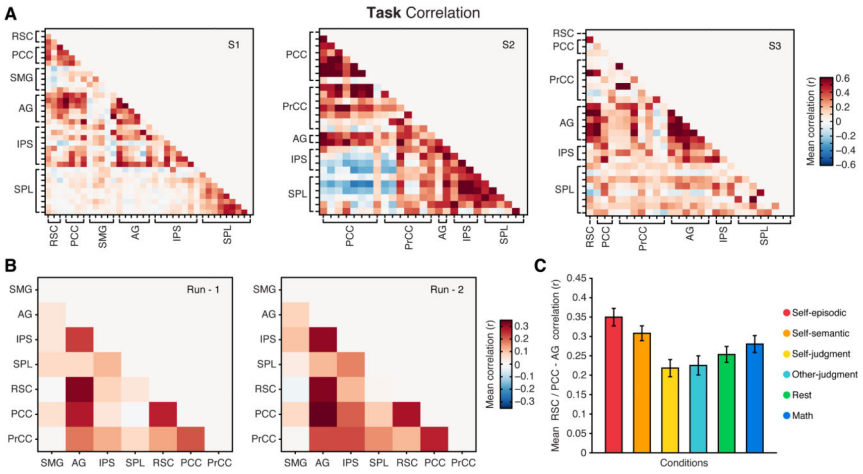

Figure 3. Consistent subregional correlation across subjects and task runs

Task correlation matrices for all parietal electrode pairs are shown for each subject (A) (correlations averaged across two task runs). B) Mean task correlation values between parietal subregions across subjects are shown for the first (left) and second (right) task runs. Correlation matrices for each task run show a highly similar pattern of correlation between regions (Run-1 vs. Run-2 matrix similarity, $r = 0.91$, $p<0.001$, $n = 21$), whereby correlations are most pronounced between RSC/PCC and AG. C) Mean RSC/PCC-AG correlation (with standard error of mean) across subjects is shown for each task condition. Mean condition correlations suggest that all task conditions comodulated RSC/PCC and AG HFB responses, with the self-episodic condition producing the greatest correlation values (main effect of condition on RSC/PCC-AG correlation $F(5, 405) = 9.11$, $p < 0.001$). See also Figure S6.

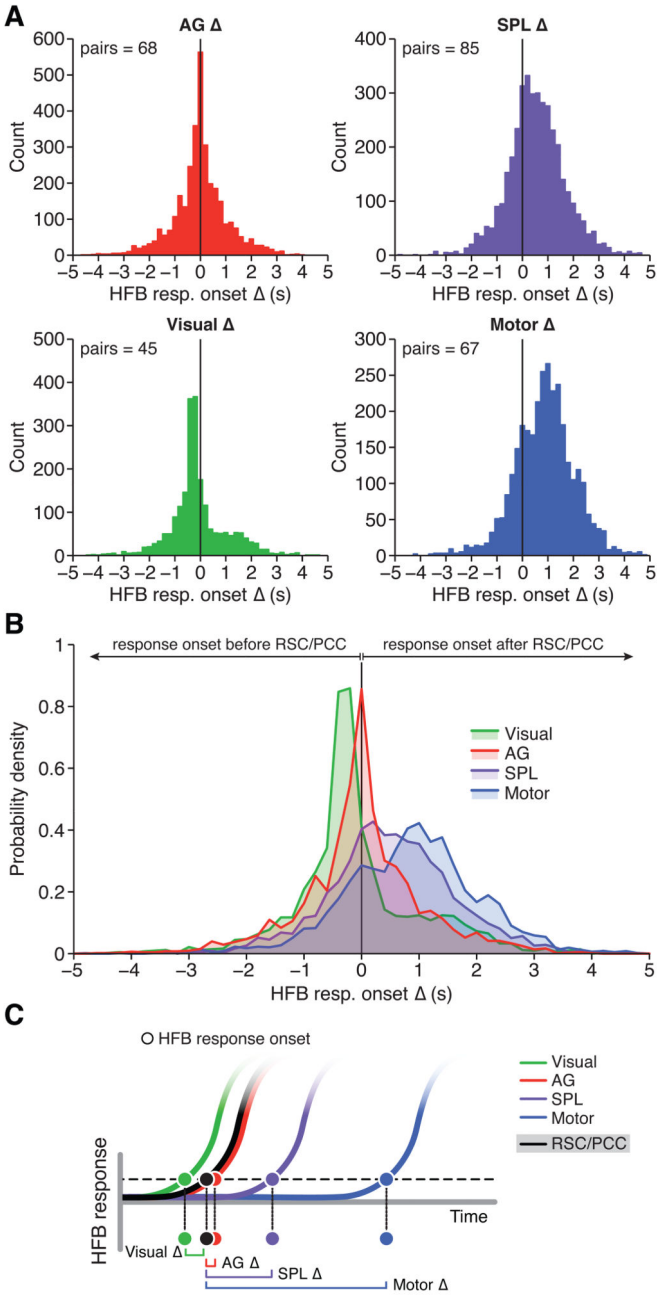

Figure 4. Relative timing of HFB response onset during episodic retrieval

A) Histograms display the distribution of HFB ROL difference latencies (i.e., ROL delay), where each region of interest is compared to RSC/PCC, for the self-episodic condition. Each observation is therefore the HFB ROL difference, for a single trial, between a given RSC/PCC site and a given AG (upper left), SPL (upper right), visual (lower left) or motor (lower right) site. B) Probability density functions for each ROL difference distribution. These distributions suggest that compared to RSC/PCC, AG showed no lag or lead bias (delay) in response onset timing, unlike other control regions. C) Schematic representation of latency distributions (A–B), which suggest a sequence of HFB response onsets during

episodic retrieval, where visual regions closely precede the near simultaneous onset of RSC/PCC and AG, followed by the engagement of SPL and finally motor cortex. See also Figures S1, S4, S5 and S6.

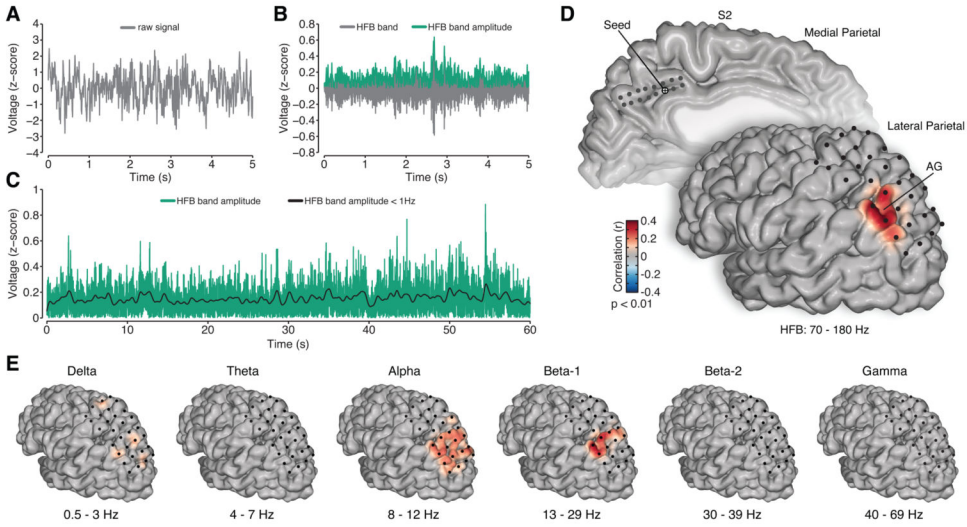

Figure 5. Resting state analysis of spontaneous ECoG data

To obtain a slow time-varying HFB signal the raw time series (A) is filtered in the HFB range (70–180 Hz) and the amplitude is extracted (B). The spontaneous HFB amplitude is then low pass filtered below 1 Hz to obtain a slow time varying HFB signal (C, example of 60 s time series from a larger 5 minute data set). D) Medial and lateral view of electrode sites in S2, with a medial PCC seed electrode highlighted, and the corresponding correlation values in lateral parietal cortex (only) interpolated onto the cortical surface. For the PCC seed, there is a selective and significant correlation with AG. E) The slow modulation of other canonical frequency bands was also studied for the same seed region. Only the low beta range (Beta-1) displayed similar, though less focal, significant correlation with AG. The significance of correlations was determined by time series permutation testing and was corrected for multiple comparisons using false discovery rate ($p < 0.01$). See also Figure S7.

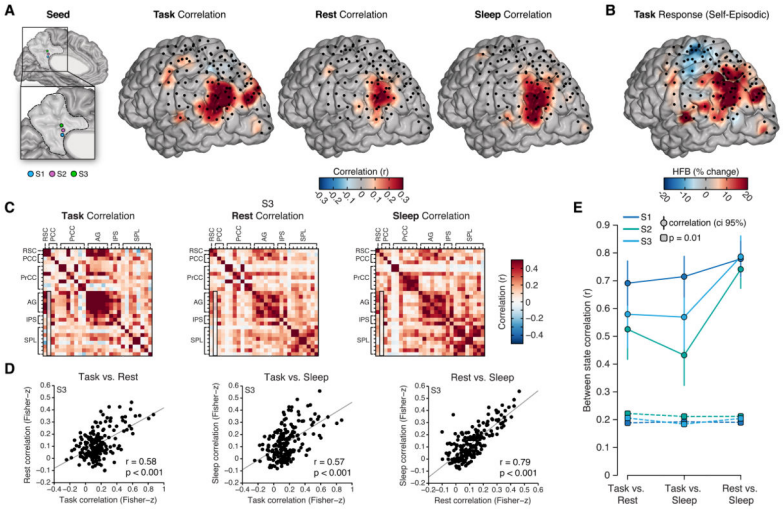

Figure 6. Similarity of ECoG correlation patterns across task, rest and sleep states

A) Correlation values for task, rest and sleep states are shown for all subjects on a shared cortical surface. Correlations are relative to a consistent RSC/PCC seed location in each subject (seed). Task data reflect trial based correlation of HFB amplitude response, whereas rest and sleep data reflect correlation of spontaneous slow (< 1 Hz) fluctuations of HFB amplitude. Across all three states, a strikingly similar pattern of correlation with the AG is observed. B) Mean HFB amplitude response (400–900 ms post stimulus onset) in LPC across all subjects during the self-episodic condition, also displays a similar pattern of activation. C) To directly compare the pattern of connectivity between task, rest and sleep states, we computed the similarity between correlation matrices across each state for each subject. Example correlation matrices are shown for S3 (note outlined column in each reflects the data used for (B); i.e., a medial seed location and all lateral site correlations). D) Scatter plots show the similarity (correlation) between states for the data shown in (C) (note: to control for correlations being driven by local within region similarity, we only included the medial-lateral correlation pairs (n = 187), e.g., AG-AG or PCC-PCC pairs excluded and PCC-AG or RSC-SPL included; see Figure S8 for all pairs). Across comparisons we see a striking positive correlation between states, which is most pronounced between rest and sleep. E) Across subjects the similarity of connectivity between states is remarkably consistent. Plot shows the between state similarity (correlation value with 95% ci) for each subject and the associated correlation value for p = 0.01 based on permutation testing (S1–S3 pairs n = 196, 180, 187). See also Figures S7 and S8.

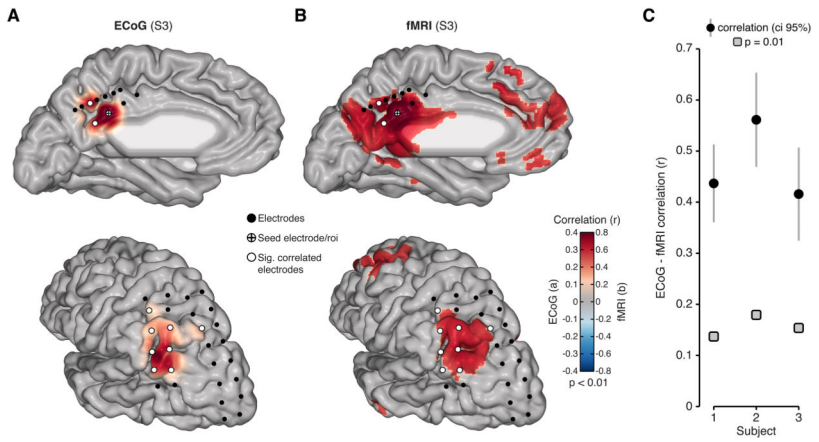

Figure 7. Similarity of ECoG and fMRI resting state connectivity

A) Resting state ECoG data is shown for an example PCC seed electrode in S3. Based on the seed region in PCC, slow (< 1 Hz) HFB amplitude is correlated significantly and selectively with AG (significant electrodes show white fill color). B) Resting state fMRI data for S3 is shown for the same seed location, but with full brain voxel wise correlation. ECoG electrode locations are overlaid to show correspondence between modalities, whereby significantly correlated electrodes co-locate with significantly correlated voxel clusters. C) For a more comprehensive and quantitative comparison, we correlated parietal connectivity matrices for rsECoG and rsfMRI data. Plot shows the correlation value and 95% confidence interval for connectivity comparisons between rsECoG and rsfMRI in each subject (gray boxes show significance level p = 0.01 based on permutation testing). Modalities were matched by extracting fMRI time series from ROI defined by each subject's electrode locations (S1–S3 pairs n = 595, 351, 378).

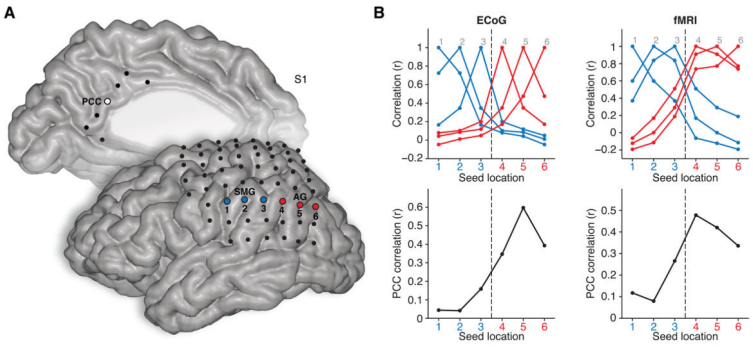

Figure 8. Similar parcellation boundaries in rsECoG and rsfMRI

A) Electrode locations for the medial and lateral surface are shown for S1 (note: electrodes beyond parietal lobe are shown for completeness). Seed electrodes of interest are highlighted for PCC (medial, white fill), SMG (lateral, blue fill) and AG (lateral, red fill). To capture an example of regional and network parcellation for both modalities, we show local and distal correlation profiles for the inferior parietal lobule (IPL, SMG→AG). B) Emulating the approach of (Cohen et al., 2008) and more recently (Wig et al., 2014), upper panels show the correlation value between each seed region (1–6) for rsECoG (left) and rsfMRI (right) data, based on the same seed locations. Both modalities display a shift in connectivity that reflects a lack of correlation (boundary) between SMG and AG, consistent with DMN organization. In addition, when comparing each IPL seed region to the target seed in PCC (lower panels), there is a strong increase in correlation values for both modalities (ECoG = left; fMRI = right) as the IPL seed location transitions into the AG, consistent with DMN organization.